

Exchange Bias and Domain Evolution at 10 nm Scales

I. Schmid,^{1,*} M. A. Marioni,^{1,†} P. Kappenberger,^{1,‡} S. Romer,¹ M. Parlinska-Wojtan,¹ H. J. Hug,^{1,§}
O. Hellwig,² M. J. Carey,² and E. E. Fullerton³

¹*Empa, Swiss Federal Institute for Materials Testing and Research, CH-8600 Dübendorf, Switzerland*

²*Hitachi Global Storage Technologies, San Jose, California 95135, USA*

³*University of California–San Diego, La Jolla, California 92093, USA*

(Received 9 February 2010; published 2 November 2010)

For a fixed $2\ \mu\text{m} \times 2\ \mu\text{m}$ area of a Co/Pt-CoO perpendicular exchange bias system we image the ferromagnetic (FM) domains for various applied fields with 10-nm resolution by magnetic force microscopy (MFM). Using quantitative MFM we measure the local areal density of pinned uncompensated spins ($p^{\text{in}}\text{UCS}$) in the antiferromagnetic (AFM) CoO layer and correlate the FM domain structure with the UCS density. Larger applied fields drive the receding domains to areas of proportionally higher $p^{\text{in}}\text{UCS}$ aligned antiparallel to FM moments. The data confirm that the evolution of the FM domains is determined by the $p^{\text{in}}\text{UCS}$ in the AFM layer, and also present examples of frustration in the system.

DOI: 10.1103/PhysRevLett.105.197201

PACS numbers: 75.30.Et, 07.79.Pk, 75.30.Gw, 75.50.Ee

It is generally believed that exchange bias (EB) implies the presence of pinned uncompensated spins $p^{\text{in}}\text{UCS}$ in the antiferromagnet (AFM) layer that are coupled to the ferromagnet (FM) layer [1]. An obstacle to understanding the EB effect is that only a subset of the UCS (those pinned and coupled to the FM) are responsible for the EB [2,3]. The experimental method and preparation may affect these subsets in distinct ways [2], and an interpretation of UCS measurements must take this into account.

Reflectometry experiments using polarized neutrons [4,5] or circularly polarized x rays [3,6] as probes have been used to access these UCS subsystems and to map out their thickness distribution. Both methods fit proposed model descriptions of these distributions to the experimental data. Neutron-based techniques can unambiguously determine the relative orientation of the UCS of the various subsystems and the FM spins. X-ray-based experiments require in addition specifying magneto-optical constants of the atomic species carrying the spin in the AFM [6] to accomplish this. Recent results have also stressed the influence on x-ray magnetic linear dichroism (XMLD) signals of the orientation of AFM spins relative to the crystallographic axes [7,8].

The reflectometry techniques currently provide only limited information on the density of pinned UCS and cannot reveal their lateral distribution. The latter extremely important aspect of EB characterizations [9] is accessible with other (complementary) techniques. Among these, photoemission electron microscopy (PEEM) with circular and/or linearly polarized x rays has revealed a correlation between AFM domains and FM domains [10], the formation of new chemical phases at the AFM-FM interface with magnetic moments parallel to those of the FM [11], and induced ferromagnetic moments at the AFM-FM interface [12,13]. Note that PEEM experiments require the applied magnetic field to be zero or near zero [14], and accordingly

cannot distinguish pinned from nonpinned UCS of the AFM [5] directly. In fact, only a small part of the net moment induced locally by the FM in the AFM consists of $p^{\text{in}}\text{UCS}$ [15], which are difficult to isolate from the rest with present-day PEEM sensitivities [13].

To date, PEEM microscopes have not attained lateral resolutions on the length scale of grain sizes of typical polycrystalline AFM materials, important for applications. Though lacking the element specificity of x-ray-based techniques, magnetic force microscopy (MFM) can reach this resolution in measurements of stray magnetic fields generated by UCS. The MFM measures shifts in the resonance frequency of a magnetic cantilever which are proportional to the prevailing magnetic field gradients. Applied uniform fields do not give rise to contrast. Likewise, no contrast is expected for a FM film of uniform thickness and magnetization, or close to the center of very wide (*vis-à-vis* the film thickness) domains, because the stray field is negligible. Such films would be “transparent” to the MFM. However, the weak field variations due to defects or the distribution of UCS in the AFM (*a priori* both of pinned and rotating type) could be detected.

Kappenberger *et al.* [16] and Schmid *et al.* [2] compared the frequency shift contrast generated by up or down FM domains with that of the pattern of $p^{\text{in}}\text{UCS}$. Under the assumption that the magnetization both within the FM domains and the corresponding areal density pattern of $p^{\text{in}}\text{UCS}$ are homogeneous, an average areal density of pinned uncompensated magnetic moments could be extracted from the measured MFM data.

In this work, we measure a $2\ \mu\text{m} \times 2\ \mu\text{m}$ area of a FM-AFM sample with MFM in various applied fields to study the evolution of appropriately designed FM domains in the presence of an adjacent AFM layer. At saturation, the calibration of the MFM tip [17] allows us to obtain the stray field generated by the AFM’s UCS density

(pinned—as will be argued) quantitatively. We developed an algorithm that avoids significant numerical errors in the deconvolution of the frequency shift data. Thus we were able to take advantage of the high lateral resolution and signal-to-noise ratio of our measurement and extract the local, i.e., position-dependent pinUCS density in the AFM. With these improvements over our work from Refs. [2,16], we can correlate the FM-domain structure with the local pinUCS density. We infer the role played by pinUCS in EB.

For this study we prepared a $\text{Pt}_{2\text{ nm}}\text{CoO}_{1\text{ nm}}\text{Co}_{0.6\text{ nm}}[\text{Pt}_{0.7\text{ nm}}/\text{Co}_{0.4\text{ nm}}]_{20}\text{Pt}_{20\text{ nm}}/\text{Si}$ structure by dc magnetron sputtering onto Si with native oxide and a 20 nm Pt buffer, as described in [18]. The anisotropy of the FM layer is perpendicular to the film surface.

With the MFM microscope we obtain the tip-sample interaction caused shift $\Delta f(x, y, z)$ of the free cantilever resonance frequency. When scanning a plane in noncontact mode at a tip-sample distance z , Δf is best described by its 2D Fourier components $\Delta f(\mathbf{k} = \{k_x, k_y\}, z)$. Then the expression

$$\Delta f(\mathbf{k}, z) = \text{ICF}(\mathbf{k}) \frac{d}{dz} H_z(\mathbf{k}, z) \quad (1)$$

relates Δf and the derivative of the magnetic field's z component, $H_z(\mathbf{k}, z)$, by a simple proportionality relation with $\text{ICF}(\mathbf{k})$, the “instrument calibration function,” determined by calibration [17].

Stray fields from the sample and the perpendicular magnetic dipoles per unit film area A that generate them [$m_z(\mathbf{k})/A$] are related by the expression [2]

$$\frac{d}{dz} H_z(\mathbf{k}, z) = -\frac{1}{2} \frac{m_z(\mathbf{k})}{A} k^2 e^{-kz}. \quad (2)$$

From Eqs. (1) and (2) it is possible to obtain $m_z(\mathbf{k})/A$ and then trivially $m_z(x, y)/A$. Note that $m_z(x, y)/A$ is a projection of the spatial density of the AFM moments on the xy plane.

At the MFM operating temperature of 8.3 K vibrating sample magnetometry [19] shows an exchange field of -30 mT upon cooling in a 1 T applied field. Conversely, no macroscopic EB is observed upon cooling in zero applied field. Nevertheless, the domain structure of the FM induces a local EB [14], and various authors [2,11–13,20] have shown that UCS patterns are formed in these conditions, mirroring the FM-domain structure present at cooling time. In Fig. 2 we address these findings.

Figures 1(a)–1(c) display high-resolution images acquired at 8.3 K of a same sample area that was cooled in $H_{\text{applied}} = 0$ starting from the as-deposited, demagnetized state, with typical maze pattern FM domains. Figure 1(a) was obtained at 0 mT, and images 1(b) and 1(c) were obtained subsequently at applied fields of 200 and 300 mT, respectively. Figures 1(d)–1(f) are the analog to (a)–(c), but prior to cooling the sample was demagnetized at room temperature with an in-plane field, which gave rise to a stripe pattern of FM domains.

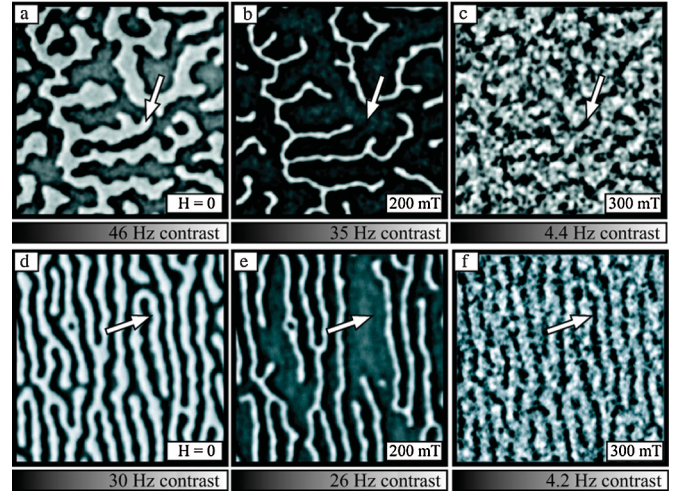


FIG. 1 (color). $2\ \mu\text{m} \times 2\ \mu\text{m}$ MFM images obtained at 8.3 K from zero applied field cooled samples: (a)–(c) are from one area cooled as deposited, at 0, 200, and 300 mT applied field, respectively. (d)–(f) are from one area cooled after in-plane demagnetization, at 0, 200, and 300 mT applied field, respectively. Arrows pointing to the same spot on the images (a)–(c) [and (d)–(f), respectively] highlight the frequency shift levels in one position at different applied fields.

The tip magnetization and the applied field are parallel in all MFM measurements presented here. Hence dark areas (“−”) correspond to parallel tip and sample magnetization; i.e., there is an attractive force and negative frequency shift. Conversely, bright areas (“+”) correspond to the antiparallel orientation.

FM domains are clearly visible in 1(a) and 1(b) and in 1(d) and 1(e), generating a Δf contrast of 46, 35, 30, and 26 Hz, respectively. As expected, the area of the bright domains (magnetization opposite to the applied field) diminishes as fields of 100 mT [19] and 200 mT are applied [Figs. 1(b) and 1(e)]. The bright domains have disappeared in Figs. 1(c) and 1(f), in agreement with magnetometry data indicating saturation at 300 mT [19].

In Figs. 1(a)–1(c) the contrast drops from 45 to 4.4 Hz as the field rises from 0 to 300 mT [from 30 to 4.2 Hz for Figs. 1(d)–1(f)]. It does not vanish, contrary to what would be expected for a uniform FM magnetization. The contrast of 4.4 Hz (4.2 Hz) is too large to be caused by reversal domains in the FM: if it were, reversal domains would account for deviations from the average (almost saturated) magnetization of the order of $4.4\ \text{Hz}/46\ \text{Hz} \approx 10\%$, which are inconsistent with the observed magnetization curve in the 300 mT to 1 T range [19]. In fact, previous work on similar films [16] already shows that reversal domains do not contribute significantly to contrast formation at saturation; see Figs. 1(c) and 1(f). Reference [16] showed that the images obtained in saturation at 800 mT, 2 T, and even after a full ± 7 T loop are essentially the same, which would not be the case if reversal domains were the cause.

In principle, a pattern of defects in the FM could govern the structure of the as-grown FM domains. Further, these defects could give rise to the formation of a matching contrast pattern at 300 mT in Figs. 1(c) and 1(f). For instance, it could cause a local change in the film saturation magnetization, or abnormal tip-sample interactions via electrostatic or van der Waals forces. However, the pattern in Fig. 1(f) bears no resemblance to Fig. 1(c), even though the putative defects would have to be equally distributed in both cases. Consequently, they are not correlated with the contrast patterns of Figs. 1(c) and 1(f), which correlate with their corresponding FM magnetization patterns at 0 mT [Figs. 1(a) and 1(d)]. This is particularly well visible for the stripe domain pattern. We discuss the relation between Figs. 1(a)–1(c) below, but must conclude at this point that the contrast in Fig. 1(c) arises from UCS of the AFM.

Because unlike PEEM images the MFM data of Fig. 1(c) and 1(f) were acquired in a magnetic field (300 mT), the UCS that rotate with the vanishing bright FM domains during the magnetization process will form a background magnetic moment density no longer reflecting the initial FM-domain pattern. Apart from local density inhomogeneities, such an UCS background will not be detectable by MFM. Hence, the main contrast is due to $p^{\text{pin}}\text{UCS}$ [19].

From the Δf pattern of Fig. 1(c) we can calculate the distribution of UCS (pinned, as discussed) using Eq. (2). The result, plotted in Fig. 2(a) (with brightness proportional to the local areal moment density and color channel according to the sign of the $p^{\text{pin}}\text{UCS}$), reveals a striking inhomogeneity of the $p^{\text{pin}}\text{UCS}$. TEM images of our films [19] show columnar grains in the film with sizes of the order of 10 nm, placing the observed $p^{\text{pin}}\text{UCS}$ variations on the same length scale. This $p^{\text{pin}}\text{UCS}$ distribution also represents an inhomogeneous distribution of “pinning” centers for FM-domain motion, leading to the commonly observed EB-induced increase in coercivity.

Figures 2(a) and 2(b) are based on Fig. 2(c) where we show the calculated $p^{\text{pin}}\text{UCS}$ density in shades of blue and yellow for each orientation. Figures 1(a) and 1(b) further have the contours of the FM domains at the indicated applied field superimposed as white lines [19]. From them we see that the $p^{\text{pin}}\text{UCS}$ in the area initially covered by “+” FM domains (bright in Fig. 1) is predominantly negative [blue in Figs. 2(a)–2(c)], whereas the areas initially covered by “–” FM domains (dark in Fig. 1) is predominantly positive [yellow in Figs. 2(a)–2(c)]. This local antiparallel alignment between the FM magnetization and the $p^{\text{pin}}\text{UCS}$ is consistent with our earlier work [2,20] and with recent work by Blackburn *et al.* using x-ray reflectometry in a permalloy/CoO FM-AFM bilayer [15]. Notice the existence of isolated regions of $p^{\text{pin}}\text{UCS}$ that do not have the same sign as the average over the FM-domain area [white arrows in Figs. 2(a) and 2(b)]. They are oriented parallel to the (initial) adjacent FM magnetization, and seem to be circumscribed to areas of the size of single grains of the film.

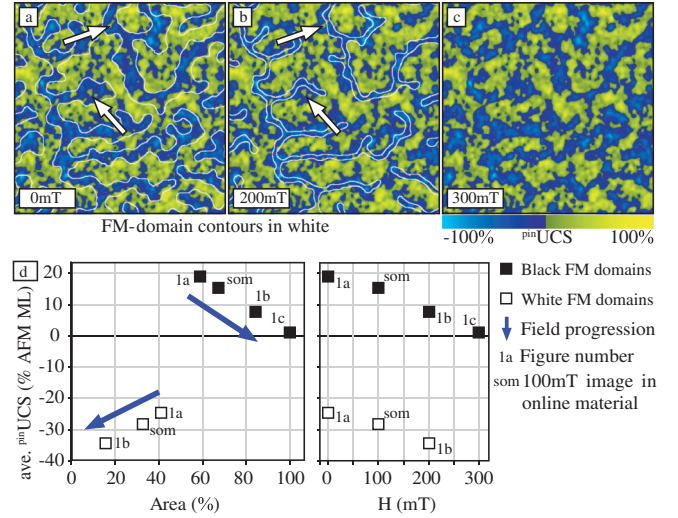


FIG. 2 (color). (a) Contours (in white) of 0 mT FM domains from Fig. 1(a) overlaid on the density of $p^{\text{pin}}\text{UCS}$ calculated from Fig. 1(c) [shades of blue and yellow for orientation opposite and parallel to the receding FM domains—white in Figs. 1(a) and 1(b)]. (b) Same as (a) for 200 mT contours. (c) Same as (a) and (b) but for $H = 300$ mT, in saturation. With few exceptions (such as pointed out by the arrows) the $p^{\text{pin}}\text{UCS}$ align antiparallel to the domain magnetization at $H = 0$. (d) Average $p^{\text{pin}}\text{UCS}$ under the domains contoured in (b) and (c), and for $H = 100$ mT [19] versus domain area (left-hand panel) and applied field (right-hand panel). The arrows in the left-hand panel indicate the field progression. The data point number indicates which figure’s domain patterns were used to compute the $p^{\text{pin}}\text{UCS}$ average.

Quantitative statements for these observations can be made by computing the average $p^{\text{pin}}\text{UCS}$ density [data from Figs. 2(a)–2(c)] for the areas delimited by the white contours of Figs. 2(b) and 2(c) corresponding to the + and – domains at 0, 100 (not shown), and 200 mT. Specifically, in $H = 0$ the average $p^{\text{pin}}\text{UCS}$ density underneath the + domains [bright in Fig. 1(a), contours in Fig. 2(b)] is $-24.6 \pm 3\%$ of a fully uncompensated monolayer of AFM spins (it is $+18.9 \pm 3\%$ under the – FM domains at $H = 0$). These values agree well with work on polycrystalline Py/CoO samples [15], which estimates the $p^{\text{pin}}\text{UCS}$ to be about 10% of a 1.1 monolayer-thick layer of interfacial Co^{2+} spins. A decreasing magnetic moment of the FM layer near the interface found in Ref. [15] may explain the somewhat smaller density of $p^{\text{pin}}\text{UCS}$ observed there. Our results are, however, in strong contrast to the UCS density obtained earlier by Ohldag *et al.* [21]. As discussed above, our experimental method evaluates the areal density of pinned UCS, rather than a depth-weighted sum of the pinned (antiparallel) and rotating (parallel) UCS [2,20]. This, however, requires that the average coupling strength between the pinned UCS and FM spins be much smaller than previously expected. Without an exhaustive theoretical analysis of the $p^{\text{pin}}\text{UCS}$ coupling strength and possible variations thereof, we point out that the interface between the AFM and the FM very likely differs from a chemically

sharp interface across which the system goes from FM to AFM. This was hinted by Ohldag *et al.* [22], who distinguished a region between the FM and the AFM where interdiffusion was important. Elsewhere in work on the subject [23], reconstruction was found in a NiO-CoFe interface. A similar reconstruction ought to be expected in the CoO/Co interfaces of this work, and may lead to a structurally and chemically disordered interfacial phase, explaining the higher density of $^{\text{pin}}\text{UCS}$ and their weaker coupling to the FM spins. In this regard, the observation of spin glass behavior of the pinned moments in FeMn/NiFe systems by Fernandez-Outon *et al.* [24] is noteworthy.

Furthermore, we carry out the above procedure also for the FM domains at 100 mT [19] and 200 mT, and plot the results in Fig. 2(d). The right-hand panel shows the effect of the applied field on the average $^{\text{pin}}\text{UCS}$ under the domains. It is clearly seen that the negative $^{\text{pin}}\text{UCS}$ adjacent to the + FM domains becomes more negative as the domains shrink at progressively higher (blue arrows) applied fields. Concurrently, the positive average $^{\text{pin}}\text{UCS}$ adjacent to the - FM domains decreases as the - domain expands. In the left-hand panel of Fig. 2(d) this evolution is seen in terms of the area covered by the FM domains. It shows that the regions of the + FM domain that last disappear as the field increases are those with negative (antiparallel coupling) $^{\text{pin}}\text{UCS}$ with the largest absolute value. In other words, at least in the CoO-Co/Pt perpendicular system, $^{\text{pin}}\text{UCS}$ s coupling antiparallel to the FM magnetization stabilize its orientation, i.e., they are *biasing*, whereas $^{\text{pin}}\text{UCS}$ s oriented parallel to the FM magnetization have the opposite effect, i.e., they are *antibiasing*. These results are a direct observation of the stabilizing effect of (antiparallel) $^{\text{pin}}\text{UCS}$ on FM domains, and show that a higher $^{\text{pin}}\text{UCS}$ density leads to a stronger FM domain pinning, i.e., a higher EB effect. Exchange coupling across AFM grain boundaries could lead to frustration of the antiparallel coupling between $^{\text{pin}}\text{UCS}$ and FM domains, giving rise to the observed antibiasing.

In conclusion, we have used MFM techniques to determine quantitatively and with 10 nm resolution the spatial distribution of the $^{\text{pin}}\text{UCS}$ density over an AFM layer in a CoO-Co/Pt exchange biased system. We correlate $^{\text{pin}}\text{UCS}$ density to the position of the ferromagnetic domains at various field levels, but on the same sample area. Thus we show without recourse to differently prepared systems that $^{\text{pin}}\text{UCS}$ aligned antiparallel to the FM magnetization

stabilize it, and parallel $^{\text{pin}}\text{UCS}$ have the opposite effect. The average $^{\text{pin}}\text{UCS}$ underneath domains of a given magnetization is roughly proportional to the applied field, proving that a higher $^{\text{pin}}\text{UCS}$ density in fact leads to stronger (local) EB.

The support from Empa, the Swiss National Science Foundation, and the NCCR Nanoscale Science of the University of Basel is hereby gratefully acknowledged.

*Present address: Comet Holding AG, CH-3175 Flamatt, Switzerland.

†Corresponding author.

Miguel.Marioni@empa.ch

‡Present address: INFICON Ltd., LI-9496 Balzers, Liechtenstein.

§Also at Department of Physics, Universität Basel, CH-4056 Basel, Switzerland.

- [1] K. Takano *et al.*, *Phys. Rev. Lett.* **79**, 1130 (1997).
- [2] I. Schmid *et al.*, *Europhys. Lett.* **81**, 17001 (2008).
- [3] S. Doi *et al.*, *Appl. Phys. Lett.* **94**, 232504 (2009).
- [4] S. Roy *et al.*, *Phys. Rev. Lett.* **95**, 047201 (2005).
- [5] M. R. Fitzsimmons *et al.*, *Phys. Rev. B* **75**, 214412 (2007).
- [6] S. Brück *et al.*, *Phys. Rev. Lett.* **101**, 126402 (2008).
- [7] E. Arenholz *et al.*, *Phys. Rev. B* **74**, 094407 (2006).
- [8] R. Abrudan *et al.* *Phys. Rev. B* **77**, 014411 (2008).
- [9] W. Kuch *et al.*, *Nature Mater.* **5**, 128 (2006).
- [10] F. Nolting *et al.*, *Nature (London)* **405**, 767 (2000).
- [11] H. Ohldag *et al.*, *Phys. Rev. Lett.* **86**, 2878 (2001).
- [12] T. Eimüller *et al.*, *Appl. Phys. Lett.* **85**, 2310 (2004).
- [13] F. Offi *et al.*, *Phys. Rev. B* **67**, 094419 (2003).
- [14] F. Offi *et al.*, *J. Magn. Magn. Mater.* **261**, 1 (2003).
- [15] E. Blackburn *et al.*, *Phys. Rev. B* **78**, 180408 (2008).
- [16] P. Kappenberger, I. Schmid, and H. Hug, *Adv. Eng. Mater.* **7**, 332 (2005).
- [17] P.J.A. van Schendel *et al.*, *J. Appl. Phys.* **88**, 435 (2000).
- [18] O. Hellwig *et al.*, *Phys. Rev. B* **65**, 144418 (2002).
- [19] See supplementary material at <http://link.aps.org/supplemental/10.1103/PhysRevLett.105.197201> for VSM, TEM, and MFM data, and a discussion of uncertainties.
- [20] P. Kappenberger *et al.*, *Phys. Rev. Lett.* **91**, 267202 (2003).
- [21] H. Ohldag *et al.*, *Phys. Rev. Lett.* **91**, 017203 (2003).
- [22] H. Ohldag *et al.*, *Phys. Rev. Lett.* **87**, 247201 (2001).
- [23] F. Allegretti *et al.*, *Surf. Sci.* **601**, L73 (2007).
- [24] L. E. Fernandez-Outon *et al.*, *J. Appl. Phys.* **104**, 093907 (2008).